Functional specificity of local synaptic connections in neocortical networks

Ho Ko[1,*], **Sonja B. Hofer**[1,*], **Bruno Pichler**[1,2], **Kate Buchanan**[1], **P. Jesper Sjöström**[1], and **Thomas D. Mrsic-Flogel**[1]

[1]Department of Neuroscience, Physiology and Pharmacology, University College London, 21 University Street, London WC1E 6DE, UK

Abstract

Neuronal connectivity is fundamental to information processing in the brain. Understanding the mechanisms of sensory processing, therefore, requires uncovering how connection patterns between neurons relate to their function. On a coarse scale long range projections can preferentially link cortical regions with similar responses to sensory stimuli[1-4]. But on the local scale, where dendrites and axons overlap substantially, the functional specificity of connections remains unknown. Here we determine synaptic connectivity between nearby layer 2/3 pyramidal neurons *in vitro* whose response properties were first characterized in mouse visual cortex *in vivo*. We found that connection probability was related to the similarity of visually driven neuronal activity. Neurons with the same preference for oriented stimuli connected at twice the rate of neurons with orthogonal orientation preferences. Neurons responding similarly to naturalistic stimuli formed connections at much higher rates than those with uncorrelated responses. Bidirectional synaptic connections were found more frequently between neuronal pairs with strongly correlated visual responses. Our results reveal the deg of functional specificity of local synaptic connections in visual cortex, and point to the existence of fine-scale subnetworks dedicated to processing related sensory information.

Paired intracellular recordings in cortical slices indicate that synaptic connectivity between neighboring neurons is heterogeneous and depends on factors such as cell type and electrophysiological properties[5-10]. In fact, even within relatively homogenous groups of neurons, connectivity is not uniformly distributed[5,6]. While this non-random connectivity raises the possibility that functionally similar neurons form synaptically coupled subnetworks[6,7], the relationship between a neuron's synaptic partners and their functional properties in local cortical circuits has not been determined.

To elucidate this relationship, we developed an approach to relate connectivity to function in identified neurons of the layer 2/3 (L2/3) network in mouse visual cortex (V1), where neurons with diverse preferences for sensory stimuli are locally intermixed[11],[12]. In anaesthetized mice, the monocular region of V1 was bulk labeled with injections of the calcium indicator dye OGB□1 AM and the astrocyte marker SR101[13] (see Methods). We first used *in vivo* two-photon imaging[14],[15] to sample spike□related somatic calcium signals from L2/3 neurons during presentation of drifting gratings and natural movie sequences (see Methods). We repeated this mapping at consecutive depths beneath the cortical surface in order to characterize visually evoked responses of all neurons within a cortical volume of approximately $285 \times 285 \times 90~\mu m^3$, starting at the upper border of L2/3 (Fig. 1a, b, depth range covered 60-120 μm). In this way, we obtained information about orientation/direction tuning and response correlation from a complete sample of L2/3 neurons (Fig. 1c, d).

We then identified the same OGB-1-filled neurons in acute slices (Fig. 1e-h, 2a) by registering image stacks obtained *in vivo* and *in vitro* using affine transformation (see Methods and Supplementary Fig. 1), and carried out simultaneous whole-cell patch clamp recordings from up to four neighboring L2/3 pyramidal neurons (mean distance $\pm$ s.d. = 25 $\pm$ 9 μm). Synaptic connectivity between cells was assessed by evoking action potentials in each neuron in turn while simultaneously recording membrane potential in the other neurons. Monosynaptic connections appeared as spike□locked postsynaptic potentials with millisecond latency (mean latency $\pm$ SEM = 1.69 $\pm$ 0.11 ms; see Fig. 2c, 3b for sample traces). This approach allowed us to determine connectivity rates and patterns (i.e. unidirectional, bidirectional), and to relate these to cell functionality in the intact brain (Fig. 1c, d, 2b, 3a).

The dataset contained imaging experiments performed on 16 mice and whole-cell recordings from 126 L2/3 pyramidal cells, 116 of which could be matched to neurons functionally characterized *in vivo* (see Methods). The rate of connectivity was 0.19 (43 connections out of 222 potential connections assayed), in keeping with previous reports[6],[8],[10]. Connection probability, synaptic strength and electrophysiological properties of OGB-1 labeled neurons were not significantly different to those recorded in slices from naive age-matched visual cortex which was not injected with OGB-1 AM (connectivity rate 0.18; 25 connected of 143 tested; Supplementary Fig. 2), indicating that dye loading, anesthesia and prolonged exposure to infra-red laser light during imaging *in vivo* did not alter these parameters.

We first examined how connectivity depended on orientation selectivity and on responsiveness to natural movies. Out of the 116 neurons, 77 were responsive to the natural movie, and 79 were orientation selective for grating stimuli (see Methods). Connection probability between orientation-tuned neurons was more than two-fold higher than among non-selective and/or non-responsive cells (0.27; 25/94 vs 0.10; 3/31; P = 0.050, Chi-square test). Connectivity rate between neurons responsive to the natural movie was significantly higher than among cells non-responsive to the movie (0.28; 30/108 vs 0.04; 2/48; P = 0.001, Chi-square test). Taken together, these data suggest that reliably responsive and feature selective neurons belong to more densely interconnected neocortical subnetworks.

We then related connection probability to neuronal preference for the angle and direction of drifting gratings (Fig. 2). For this analysis, we only included pairs in which both neurons were responsive (74/113), orientation selective (OSI > 0.4; 53/74), or direction selective (DSI > 0.3; 41/53; see Methods and Supplementary Fig. 3a-c). Connectivity rate decreased with increasing difference in orientation preference (P = 0.040, Cochran-Armitage test for trend, Figure 2d). For similarly tuned cells, connection probability was high (0.38; 10/26; ΔORI < 22.5°), more than two-fold higher than for cells with a large difference in orientation preference (0.17; 4/24; ΔORI > 67.5°). Thus, neuronal pairs similarly tuned for

orientation were more likely to connect to each other, although a considerable connectivity rate was still observed between neurons tuned to dissimilar or orthogonal orientations. These results are consistent with the narrow suprathreshold yet broader subthreshold tuning for orientation and direction in mouse V1 neurons[16]. The same decrease of connection probability with increase in ΔOri was found for direction selective pairs (P = 0.034, Cochran-Armitage test, Fig. 2e), but these neurons only connected specifically with respect to orientation not preferred direction (Fig. 2e). These data suggest that directional preference is not conferred by biased local excitatory input, so other cell intrinsic or network mechanisms (e.g., biased long range input, specific inhibition) may be needed to explain the emergence of direction selectivity. Varying the criteria for orientation or direction selectivity (OSI/DSI from 0.2 to 0.6) did not change the dependence of connectivity on difference in orientation/direction preference (Supplementary Fig. 3d, e), suggesting that neurons which are broadly or sharply tuned both tend to connect preferentially to others with similar functional preference. In our dataset we did not find evidence suggesting that neurons with similar preferred orientation or direction are connected by stronger (EPSP amplitude) or more facilitating (paired-pulse ratio, PPR) connections than neurons with different preferred orientation or direction (Supplementary Fig. 4a, b, d and e; also see Supplementary Fig. 5 for a sample pair with strong connections), although the sample size may not be adequate for ruling out any subtle trends.

The visual cortical circuit is constantly engaged in processing natural scenes, so statistical dependencies between neuronal activities in the presence of such stimuli may reflect connectivity. We therefore tested how network connectivity relates to the similarity of neuronal responses during presentation of stimuli with natural spatiotemporal statistics (Figure 3, see Methods). For each neuronal pair in which both neurons responded reliably to natural movies (56/113), we computed the time-varying firing-rate correlation of average responses (signal correlation) to repeated presentations of a 30 to 40-second-long natural movie sequence (Fig. 3a). On average, signal correlations were low (mean ± s.d. = 0.08 ± 0.10). The probability of finding a connection between two neurons significantly increased with signal correlation to natural movies (P = 0.0002, Cochran-Armitage test, Fig. 3c). For pairs with close to zero or weakly negative signal correlation (<0.05), the connection probability was low (0.11, 5/44). In contrast, for neuronal pairs with stronger signal correlation (>0.15), the connection probability was more than four-fold higher (0.5; 13/26). Therefore, connectivity in mouse visual cortex is highly selective with respect to neuronal responses to natural movies. EPSP amplitude and paired-pulse ratio, however, were not found to change significantly with increase in signal correlation (Supplementary Fig. 4c, f; also see Supplementary Fig. 5), although the sample size may not be large enough to rule out subtle trends.

Correlated variability in neuronal firing independent of a sensory stimulus is assumed to reflect neuronal connectivity in the network[17-19]. Correlated fluctuations in neuronal firing may either be driven by common input or by recurrent synaptic connections, or both. For a subset of visually responsive neuronal pairs (12/56) that were imaged simultaneously *in vivo* (i.e. on the same optical planes), we computed noise correlations (see Methods), which provide an indication of correlated response variability. Noise correlations were low (mean ± s.d. = 0.02 ± 0.04). Despite the small sample size, connection probability was found to increase significantly with increase in noise correlation (Fig. 3d, P = 0.011, Cochran-Armitage test), indicating that recurrent connectivity may contribute to correlated fluctuations of neuronal firing.

We next compared how visual response similarity relates to connectivity motifs in the local network. Previous work indicates that bidirectional connections are over-represented in a network of sparsely connected pyramidal neurons[5]. We found that the connectivity bias

between neurons responding similarly to drifting gratings or to natural movies was further accentuated when investigating the distribution of unidirectionally or bidirectionally connected pairs (Fig. 4). We found a decreasing trend relating probability of bidirectional connections and difference in orientation preference (Fig. 4a, b; P = 0.070 for all orientation selective pairs; P = 0.036 for direction selective pairs, Cochran-Armitage test). Importantly, the monotonic fall-off in the incidence of bidirectional motifs was steeper than the overall decrease in probability of finding connected pairs as ΔOri increased (Fig. 4a, b). Similarly, the incidence of bidirectional connections increased sharply as signal correlation to natural movies increased (P = 0.003, Cochran-Armitage test, Fig. 4c), such that signal correlation was almost three-fold higher for recurrently connected pairs than unconnected pairs (mean signal correlation of bidirectionally connected pairs ± s.d. = 0.16 ± 0.07 vs 0.06 ± 0.10 for unconnected pairs; P = 0.01, rank sum test). Since probability of unidirectionally connected pairs did not show a monotonic trend with increase in response similarity (Fig. 4a-c, P > 0.4 for all conditions, Cochran-Armitage test), reciprocal connectivity reflects functional similarity better than does unidirectional connectivity.

In this study, we have characterized the functional specificity of local connections in mouse V1. Our results demonstrate that connectivity between neighboring neurons (<50 μm apart) is not random, but specifically structured; visually driven neurons were more likely to connect to each other, and this probability increased with the degree of their response similarity. This relationship between connectivity and function was stronger when comparing responses to natural sensory input than for relatively artificial grating stimuli.

We have shown in mouse V1 that—although a given neuron receives input from nearby neurons preferring a wide range of stimulus orientations—more than twice as many connections are made between similarly tuned neurons as between disparately tuned cells. In keeping, subthreshold tuning in L2/3 pyramidal neurons in mouse V1 is broad but nonetheless biased towards the preferred orientation[16]. This is similar to the tuning of neurons in pinwheel centers of orientation maps in visual cortex of other species[20]. In carnivores and primates, long-range horizontal projections in L2/3 (>500 μm) are biased towards cortical columns with similar orientation preference[1-4]. Our results indicate that similar principles of connectivity apply at the level of local neocortical networks in the mouse—a species without columnar architecture—suggesting that functionally biased connectivity may be a general feature of organization in the visual cortex. In the visual cortex this selective connection scheme may serve as mechanism for amplification of thalamic input and sharpening of tuning[21,22] or for local contour integration[23].

Analysis of connectivity rate with respect to similarity of responses to natural movies revealed a striking degree of specificity of local connections (Fig. 3c, d). Connection probability increased sharply with increase in both signal and noise correlation to natural movies. Neurons with higher signal correlation to natural movies likely share similar receptive field structure, and may therefore be driven by common feed-forward input[24]. Our results are therefore consistent with the finding that L2/3 pyramidal neurons form highly interconnected subnetworks sharing common input from layer 4 in slices of rat visual cortex[6]. Developmentally, this organization of lateral connections based on receptive field similarity may arise through activity-dependent synaptic plasticity, whereby neurons driven by common input develop stable bidirectional connections[25]. Indeed, our data show that the majority of bidirectionally connected neurons had stronger signal correlations to natural movies and shared similar orientation preference. Since individual neurons exhibit variability in their responses to the same visual stimulus[26], recurrent excitation between similarly tuned neurons may reduce response variance, while introducing redundancy into the population code for robustness against errors[27].

Our results do not preclude the possibility that other factors—including gap junction coupling, inhibitory connections or synaptic strength—also contribute to functional specificity in the circuit. Since inhibition, in particular, may be important in determining the receptive field properties of neurons in V1[28], it will be important to examine the extent to which inhibitory connections are functionally specific[7].

In conclusion, by using a novel and relatively straightforward approach for *in vitro* mapping of synaptic connectivity among neurons that had been identified functionally *in vivo*, we found that neighboring neurons with similar feature selectivity preferentially but not exclusively connected to each other in L2/3 of mouse V1. Together with other powerful approaches[29],[30], our method can be used to uncover functional biases of connectivity between different cell types and cortical layers, and in other brain areas. This information will be critical for understanding the functional wiring of circuits mediating perception and behavior.

Methods Summary

Anaesthetized C57Bl/6 mice between postnatal day 22 and 26 were injected with the calcium-sensitive dye Oregon Green Bapta-1 AM into monocular V1 as described previously[11] and in vivo two-photon calcium imaging[14],[15] was used to record responses of layer 2/3 neurons to 8 different drifting square-wave gratings (0.035 cycles/degree, 2 cycles/s, 100% contrast) and natural movie sequences. Spike trains were inferred from calcium signals using a non-negative deconvolution method. Preferred orientation and direction, as well as orientation selectivity index (OSI) and direction selectivity index (DSI) were calculated using Fourier-interpolated tuning curves. Pearson's correlation coefficient was used to obtain pair-wise response correlations, either from average responses to the stimulus (signal correlation) or from mean-subtracted responses (noise correlation). Small volumes of fluorescent microspheres were injected into the imaged region to facilitate identification of the region in the sliced brain. Coronal slices were cut after dissection of the brain, and whole-cell recordings from up to four cells simultaneously were carried out in the vicinity of the microsphere tract (identified by two-photon microscopy). The presence of synaptic connections was tested by evoking five spikes at 30-Hz in each cell, repeated for 30-90 times. Connection probability is the number of detected connections over the total number of potential connections assayed. Probability of finding uni- or bidirectionally connected pairs was calculated as the number of uni- or bidirectionally connected pairs over the total number of pairs. To register *in vivo* and *in vitro* image stacks and to match the same neurons imaged *in vivo* and recorded from *in vitro*, three-dimensional image registration by affine transformation using custom-written MATLAB software was performed subsequent to the experiment. To relate connectivity to functional properties, the asymptotic Cochran-Armitage test for trend was used to test for significance.

Supplementary Material

Refer to Web version on PubMed Central for supplementary material.

Acknowledgments

Appendix

Methods

Animals and surgical procedures

All experimental procedures were carried out in accordance with institutional animal welfare guidelines and were licensed by the UK Home Office. Experiments were performed on C57Bl/6 mice between P22-26, when both intrinsic and visually driven cortical responses exhibit a relatively mature phenotype[31],[32]. Mice were initially anesthetized with a mixture of Fentanyl (0.05 mg/kg), Midazolam (5.0 mg/kg), and Medetomidin (0.5 mg/kg). Light anesthesia was maintained during recordings by isoflurane (0.3-0.5%) in a 60:40% mixture of O_2:N_2O delivered via a small nose cone. Surgery was performed as described previously[11]. Briefly, a small craniotomy (1-2 mm) was carried out over primary visual cortex and sealed after dye injection with 1.6% agarose in HEPES-buffered ACSF and a cover slip.

Dye loading and two-photon calcium imaging in vivo

For bulk loading of cortical neurons, the calcium-sensitive dye Oregon Green Bapta-1 AM (OGB-1 AM, Molecular Probes) was first dissolved in 4 µl DMSO containing 20% Pluronic, and further diluted (1/11) in dye buffer (150 mM NaCl, 2.5 mM KCl, and 10 mM HEPES [pH 7.4]) to yield a final concentration of 0.9 mM. Sulforhodamine 101 (SR101, 50 µM, Molecular Probes) was added to the solution to distinguish astrocytes from neurons[13]. The dye was slowly pressure injected into the right visual cortex at a depth of 150-200 µm with a micropipette (3-5 MΩ, 3-10 psi, 2-4 min) under visual control by two-photon imaging (10x water immersion objective, Olympus). Activity of cortical neurons was monitored by imaging fluorescence changes with a custom-built microscope and a mode-locked Ti:sapphire laser (Mai Tai, Spectra-Physics) at 830 nm through a 40× water immersion objective (0.8 NA, Olympus). Scanning and image acquisition were controlled by custom software written in LabVIEW (National Instruments). The average laser power delivered to the brain was <50 mW.

Imaging frames of 256×256 pixels were acquired at 7.6 Hz, starting at ~110 µm below cortical surface, corresponding to superficial layer 2 in mouse V1. After each recording, the focal plane and imaging position was checked and realigned with the initial image if necessary. To obtain visually evoked responses from all neurons in a cortical volume of approximately 285×285×60-120 µm³, images were recorded at 9 to 18 cortical depths with a spacing of 7 µm. At the end of each experiment, fluorescent microspheres (Lumafluor, FL) were carefully pressure-injected into the imaged volume with a glass-pipette, resulting in small fluorescent landmarks (5-20 µm diameter) along the pipette track. These landmarks were used to assist in subsequent identification of the imaged region in the sliced brain (see below), as well as fine-scale registration of *in vivo* and *in vitro* image stacks.

Visual stimulation

Visual stimuli were generated using MATLAB Psychophysics Toolbox[33],[34], and displayed on a LCD monitor (60 Hz refresh rate) positioned 20 cm from the left eye, roughly at 45 degree to the long axis of the animal, covering ~105×85 degrees of visual space. At the beginning of each experiment, the appropriate retinotopic position in visual cortex was determined using small grating stimuli at 12-24 neighboring positions. Only cortical regions in the monocular part of primary visual cortex were included in the analysis. The monitor was repositioned such that the preferred retinotopic position of most imaged neurons was roughly in the middle of the monitor. Calcium signals were measured in response to sequences of full-field grating stimuli and natural movies. Square wave gratings (0.035

cycles/degree, 2 cycles/s, 100% contrast) drifting in eight different directions were randomly interleaved, with the grating standing for 1.4-1.9 s before moving for 0.9-1.5 s (6 repetitions per grating). Naturalistic movies consisted of 30 or 40 second sequences of moving scenes compiled from David Attenborough's Life of Mammals (BBC) and cage scenes from a head-mounted mouse camera, adjusted to 70% mean contrast (repeated 4-7 times).

Analysis of calcium signals

Image sequences were aligned for tangential drift and analyzed with custom programs written in ImageJ (NIH), MATLAB (Mathworks) and LabVIEW. Recordings with significant brain movements, vertical drift, or both were excluded from further analysis. Outlines of neurons recorded were semi-automatically defined using software written in MATLAB (Mathworks). All pixels within each ROI were averaged to give a single time course ($\Delta F/F$), which was additionally high-pass filtered at a cut-off frequency of 0.02 Hz to remove slow fluctuations in the signal.

Spike trains were inferred from calcium signals using a fast non-negative deconvolution method which approximates the *maximum a posteriori* spike train for each neuron, given the fluorescence observations[35]. Performance of the algorithm was tested by cell-attached recordings performed simultaneously with calcium imaging. There was a close correspondence between inferred and recorded spike rates (mean correlation ± s.d. = 0.82 ± 0.06; 9 cells from 4 animals).

Visual responsiveness was determined by the following procedure: For all stimulus repetitions, inferred spike trains were moving-average filtered with a time window of 3 frames (~0.394 s). The smoothed firing rates at corresponding points of the stimulus were then treated as groups and tested for differences by one-way ANOVA. Neurons with P-value less than 0.05 were considered visually responsive. This allowed neurons that exhibited consistent elevated firing during at least one period of stimulus presentation to be detected. Among cells responsive to grating stimuli, sum of firing rates of 8 frames (~1.05 s) 0.13 s after onset of grating drift was taken as the response to each stimulus. Responses from different trials were averaged to obtain the orientation tuning curve. This orientation tuning curve was then Fourier interpolated to 360 points, and the preferred direction was determined by the angle at which the interpolated tuning curve attained its maximum. The preferred orientation was taken as the modulus of the preferred direction to 180 degrees. Orientation selectivity index (OSI) was calculated as $(R_{best}-R_{ortho})/(R_{best}+R_{ortho})$, where R_{best} is the interpolated response to the best direction, and R_{ortho} is the average of interpolated responses to the directions orthogonal to best responding direction. Direction selectivity index (DSI) was calculated as $1-R_{null}/R_{best}$, where R_{null} is the interpolated response to the angle opposite the best responding direction. When relating connection probability to orientation selectivity or direction selectivity, neurons were defined to be orientation selective if OSI > 0.4, and direction selective if DSI > 0.3. Varying these criteria from 0.2 to 0.6 did not change the results (Supplementary Fig. 3). We used Pearson's correlation coefficient to obtain pairwise response correlations for cell pairs, using estimated spike rates. Signal correlation was calculated as the correlation coefficient of the average responses to stimulus. Noise correlation was found by subtracting the average response from the responses to each trail, and then calculating the correlation coefficient of mean-subtracted responses.

In vitro whole-cell recording

We carried out imaging experiment on a total of 16 mice which were followed by patch clamp recordings *in vitro*. After the functional properties of individual neurons had been determined *in vivo* by two□photon calcium imaging, the mouse brain was rapidly removed

to and dissected in ice-cold artificial cerebrospinal fluid (ACSF) containing 125 mM NaCl, 2.5 mM KCl, 1 mM $MgCl_2$, 1.25 mM NaH_2PO_4, 2 mM $CaCl_2$, 26 mM $NaHCO_3$, 25 mM Dextrose; osmolarity 315-325 mOsm, bubbled with 95% O_2/5% CO_2, pH 7.4. Visual cortex slices (300 µm) were cut coronally (HM 650 V Vibration Microtome, MICROM) and were incubated at 34 °C for thirty minutes before they were transferred to the recording chamber. The slice containing the imaged region was identified by the presence of OGB-1 green fluorescence and the red microsphere injection site. To reveal the relative locations of cells, a detailed morphological stack of the slice was acquired with a custom-built microscope and a mode-locked Ti:sapphire laser (Chameleon, Coherent) at 830 nm through a 16× water immersion objective (0.8 NA, Nikon). Scanning and image acquisition were controlled by custom software written in LabVIEW (National Instruments). Whole cell recordings from up to four cells were carried out in regions identified by visually comparing image stacks obtained *in vivo* and *in vitro*, using red fluorescent microspheres and the pial surface as reference. At this point, the experimenter was blind to the functional identity of the recorded neurons. Recordings were carried out in 28°C ACSF, using Multiclamp 700B amplifiers (Axon Instruments) and data was acquired using custom software[36] running in Igor Pro (WaveMetrics Inc.). Recording pipettes were filled with internal solution containing 5 mM KCl, 115 mM K-Gluconate, 10 mM K-HEPES, 4 mM MgATP, 0.3 mM NaGTP, 10 mM Na-Phosphocreatine, 0.1% w/v Biocytin, 40 µM Alexa Fluor 594; osmolarity 290–295 mOsm, pH 7.2. The chloride reversal potential was ~−85.2 mV. Junction potential was not corrected for. Cells were approached under visual guidance using laser-scanning Dodt contrast. After break-through, the presence of synaptic connections was tested using five suprathreshold 5-ms-long current pulses delivered as 30-Hz trains into each cell sequentially while monitoring for postsynaptic responses in the other cells, repeated at least 30 times at 15-second intervals. Postsynaptic traces were averaged, and monosynaptic excitatory connections were deemed present when there were action potential-locked depolarizing postsynaptic potentials associated with all five presynaptic spikes that exhibited millisecond latency[37]. Latency was measured as the time between the peak of the action potential and 5% of the EPSP. If no spike-locked depolarizing postsynaptic potentials were present, up to 60 additional repetitions were acquired to ensure the absence of a post-synaptic response. With this approach, unitary EPSPs as small as 0.015 mV have been reported previously[5], the smallest EPSP in the present dataset was 0.035 mV. PPR was calculated as the amplitude of the second evoked EPSP over that of the first one. Input resistance was monitored throughout recordings by measuring the steady-state membrane potential change due to brief −25 pA current injections. After connectivity mapping, step currents from −50 pA to 700 pA were injected at 50 pA increments and spike threshold was measured from the inflexion point of the minimally suprathreshold trace. Spike height was the difference between spike threshold and peak. Spike half-width was measured at the mean of threshold and peak. Pyramidal neurons were identified according to morphology in Alexa 594 filled image stacks (Fig. 2a), electrophysiological properties (resting membrane potential ~−80mV, spike half-width > 1ms, spike height ~80mV, regular spiking pattern typical of pyramidal neurons with current injection, see Supplementary Fig. 2c-e) and, in the presence of connections, depolarizing postsynaptic potentials (Fig. 2c, 3b).

Registration of in vivo and in vitro image stacks

In order to accurately match up *in vivo* and *in vitro* image stacks and to locate neurons of known *in vivo* functional preference, three□dimensional image registration using custom-written MATLAB software was performed after patch clamp experiments. The two stacks containing the same region to be matched differ in rotation and translation, as well as scales along axes. In other words, taking the center of each stack as origin, same points in the two stacks can be related by affine transformation. This can be written as

$$\vec{y} = A\vec{x} + \vec{b}$$

Where $\vec{x}$ and $\vec{y}$ are column vectors of coordinates in *in vivo* and *in vitro* stack, respectively **A**, is a 3×3 matrix representing linear transformation, and $\vec{b}$ is the translation. To find the affine transformation four pairs of corresponding points, $(\vec{x_1 y_1})$, $(\vec{x_2 y_2})$, $(\vec{x_3 y_3})$ and $(\vec{x_4 y_4})$, were manually picked from the stacks, using landmarks such as blood vessel bifurcations, fluorescent bead injections, cortical surface, and/or brightly labeled astrocytes. The relationship between the first pair of points $(\vec{x_1 y_1})$ is

$$\vec{y_1} = A\vec{x_1} + \vec{b}$$

$$\vec{b} = \vec{y_1} - A\vec{x_1}$$

Substitute this into

$$A\left[\vec{x_2}\vec{x_3}\vec{x_4}\right] + \left[\vec{b} \quad \vec{b} \quad \vec{b}\right] = \left[\vec{y_2}\vec{y_3}\vec{y_4}\right]$$

and let $\vec{x_t}' = \vec{x_t} - \vec{x_1}$, $\vec{y_t}' = \vec{y_t} - \vec{y_1}$ where $i = 2, 3, 4$, gives

$$A\left(\left[\vec{x_2}\vec{x_3}\vec{x_4}\right] - \left[\vec{x_1}\vec{x_1}\vec{x_1}\right]\right) = \left[\vec{y_2}\vec{y_3}\vec{y_4}\right] - \left[\vec{y_1}\vec{y_1}\vec{y_1}\right]$$

$$A\left(\left[\vec{x_2}'\vec{x_3}'\vec{x_4}'\right]\right) = \left[\vec{y_2}'\vec{y_3}'\vec{y_4}'\right]$$

$$A\left(\left[\vec{y_2}'\vec{y_3}'\vec{y_3}'\right]\right)\left(\left[\vec{x_2}'\vec{x_3}'\vec{x_3}'\right]\right)^{-1}$$

Knowing the linear transformation **A**, $\vec{b}$ can also be found.

In practice, to assist the process of identifying corresponding points, after picking three pairs of points, the image stacks were both rotated such that the planes containing the three pairs of points became parallel to the xy-plane, and the *in vitro* stack was further transformed such that the stacks became roughly registered in 2D on the planes but not along the z-axis (Supplementary Fig. 1a, b). To do this, let R_v and R_t are the matrices for rotating *in vivo* and *in vitro* stacks respectively, and let $\vec{u} = \left[u_x u_y u_z\right]^T$ be a unit vector, the matrix for rotating a point around $\vec{u}$ by angle θ (right handedly) is given by

$$R = \begin{bmatrix} 0 & -u_z & u_y \\ u_z & 0 & -u_x \\ -u_y & u_x & 0 \end{bmatrix} \sin\ \theta + \left(I - \vec{u}\,\vec{u}^T\right)\cos\theta + \vec{u}\,\vec{u}^T$$

where **I** is the identity matrix. To rotate the *in vivo* stack such that the plane containing the first three points picked becomes parallel to the xy-plane, the vector and the angle are

$$\vec{u_v} = \frac{\left(\vec{x_2'} \times \vec{x_3'}\right) \times \vec{e_z}}{\left\| \left(\vec{x_2'} \times \vec{x_3'}\right) \times \vec{e_z}\right\|}$$

$$\theta_v = \cos^{-1}\left(\frac{\left(\vec{x_2'} \times \vec{x_3'}\right) \cdot \vec{e_z}}{\|\vec{x_2'} \times \vec{x_3'}\|}\right)$$

where $\vec{e_z} = [0\quad 0\quad 1]^T$, × denotes cross product, · denotes dot product and $\|\quad\|$ denotes norm. Substituting these into the formula for rotation matrix above, we can find $\mathbf{R_v}$, and similarly $\mathbf{R_t}$ can also be found. To register the two planes in 2D, a further linear transformation parallel to xy-plane can be applied to the *in vitro* stack. Let $\vec{x'_{tR}}$ be the x, y components of $R_v\vec{x'_v}$, and $\vec{y'_{tR}}$ be the x, y components of $R_t\vec{y'_t}$, where $i = 2,3$, the matrix **M** needed for the 2D transformation is given by

$$M\left[\vec{y'_{2R}}\,\vec{y'_{3R}}\right] = \left[\vec{x'_{2R}}\,\vec{x'_{3R}}\right]$$

$$M = \left[\vec{x'_{2R}}\,\vec{x'_{3R}}\right]\left[\vec{y'_{2R}}\,\vec{y'_{3R}}\right]^{-1}$$

Therefore, the transformation $\mathbf{T_t}$ applied to the *in vitro* stack is

$$T_t = \begin{bmatrix} M & 0 \\ 0 & 1 \end{bmatrix} R_t$$

After this step, we picked one more pair of corresponding points from a plane different from the plane that contained the initial three pairs of points (Supplementary Fig. 1b, lower panel), which is necessary for $\left[\vec{x_2}\vec{x_3}\vec{x_4}\right]$ and $\left[\vec{y_2}\vec{y_3}\vec{y_4}\right]$ to be invertible, **A** can then be found and be applied to the *in vivo* stack. With the affine transformation known, we could find the correspondence between points. When rotating or transforming the images stacks, trilinear

interpolation was used to assign pixel values. After registration, we inspected several planes of the transformed stack containing neurons recorded *in vitro* and made use of three-dimensional relationships of nearby cells to visually verify the matching (cf. Fig 1g, h, Supplementary Fig. 1c). Among 126 pyramidal neurons patched, matching was successful for 116 while 10 failed: 3 cells were occluded in the *in vivo* stack by a blood vessel, and 7 cells did not show convincing matching in 3D on visual inspection.

Analysis of connection probabilities

Connection probabilities were calculated as the number of connections detected over the number of potential connections assayed. For example, with one quadruplet there are $4 \times 3 = 12$ potential connections, and if two connections were detected the corresponding figure would be 2/12. Probability of unidirectional and bidirectional connections were calculated as the number of unidirectionally and bidirectionally connected pairs over the total number of pairs respectively. To relate connectivity to functional properties, the asymptotic Cochran-Armitage test for trend was used to test for significance[38]. Scores of [2, 1, 0] and [2, 1, 0, 1, 2] were used in the test to relate connection probability or probability of finding bidirectionally connected pairs to increase in ΔOri among orientation selective pairs and direction selective pairs, respectively. Scores of [0, 1, 2, 3, 4] were used to relate connection probability or probability of finding bidirectionally connected pairs to the increase in signal correlation. To related connection probability to increase in noise correlation, scores of [0, 1, 2] were used.

Criteria for inclusion in data analysis

After patching, image stacks of patched neurons filled with Alexa 594 were taken and coordinates of approximate centers of neuronal somata were manually picked in a custom-written MATLAB program. The distance between slice surface right above the patched neuron and the soma center was taken as the depth of neuron from slice surface. Only neuronal pairs in which both neurons were located at >60 μm depth and with an inter-soma distance of <50 μm were included in the analysis relating connectivity to visual functional properties. On average we patched 7.9 neurons (range: 2-14) and assayed 13.9 potential connections (range: 2-31) per slice for neuronal pairs located deeper than 60 μm in the slice and separated by less than 50 μm.

Neuronal pairs closer to slice surface are more likely to have connections severed, and we found a significant increase in probability of finding connections with depth of potential presynaptic neuron (P = 0.043, Cochran-Armitage test) or postsynaptic neuron (P = 0.041, Cochran-Armitage test) (Supplementary Fig. 6a, b). However, inclusion of cell pairs closer to slice surface (which increases false negative rate of connection detection), or increasing the depth criteria (which reduces sample size) in analysis did not change the main findings (Supplementary Fig. 6d-f). Between neuronal pairs located deeper than 60 μm from slice surface, 222 connections were assayed between pairs separated by less than 50 μm. We did not find a significant difference in connection probability for neuronal pairs separated by less than 25 μm compared to those spaced farther apart (P = 0.594, Chi-square test, Supplementary Fig. 6c).

In 18 out of 113 pairs, high quality recording were achieved in one cell only (e.g. the other cell was very depolarized/unhealthy, or the seal resistance was less than 1 GΩ). Since action potentials could still be evoked in both neurons, these pairs were included as pairs in which connectivity was assayed in the direction from the unhealthy cell to the healthy cell only. Data from these pairs were included in the analysis of connection probability, but not in the analysis of probability of finding bidirectional or unidirectional pairs. Analysis of intrinsic electrophysiological properties was carried out only if series resistance was less than 30 MΩ.

References Methods

31. Smith SL, Trachtenberg JT. Experience-dependent binocular competition in the visual cortex begins at eye opening. Nat. Neurosci. 2007; 10:370–375. [PubMed: 17293862]

32. Rochefort NL, et al. Sparsification of neuronal activity in the visual cortex at eye-opening. Proc. Natl. Acad. Sci. U.S.A. 2009; 106:15049–15054. [PubMed: 19706480]

33. Brainard DH. The Psychophysics Toolbox. Spat Vis. 1997; 10:433–436. [PubMed: 9176952]

34. Pelli DG. The VideoToolbox software for visual psychophysics: transforming numbers into movies. Spat Vis. 1997; 10:437–442. [PubMed: 9176953]

35. Vogelstein JT, et al. Fast non-negative deconvolution for spike train inference from population calcium imaging. J Neurophysiol. 2010 doi:10.1152/jn.01073.2009.

36. Sjöström PJ, Turrigiano GG, Nelson SB. Rate, timing, and cooperativity jointly determine cortical synaptic plasticity. Neuron. 2001; 32:1149–1164. [PubMed: 11754844]

37. Debanne D, et al. Paired-recordings from synaptically coupled cortical and hippocampal neurons in acute and cultured brain slices. Nat Protoc. 2008; 3:1559–1568. [PubMed: 18802437]

38. Agresti, A. Categorical Data Analysis. Second Edition. Wiley InterScience; 2002.

References

1. Bosking WH, Zhang Y, Schofield B, Fitzpatrick D. Orientation selectivity and the arrangement of horizontal connections in tree shrew striate cortex. J. Neurosci. 1997; 17:2112–2127. [PubMed: 9045738]

2. Gilbert CD, Wiesel TN. Columnar specificity of intrinsic horizontal and corticocortical connections in cat visual cortex. J. Neurosci. 1989; 9:2432–2442. [PubMed: 2746337]

3. Roerig B, Kao JP. Organization of intracortical circuits in relation to direction preference maps in ferret visual cortex. J. Neurosci. 1999; 19:RC44. [PubMed: 10594088]

4. Weliky M, Kandler K, Fitzpatrick D, Katz LC. Patterns of excitation and inhibition evoked by horizontal connections in visual cortex share a common relationship to orientation columns. Neuron. 1995; 15:541–552. [PubMed: 7546734]

5. Song S, Sjöström PJ, Reigl M, Nelson S, Chklovskii DB. Highly nonrandom features of synaptic connectivity in local cortical circuits. PLoS Biol. 2005; 3:e68. [PubMed: 15737062]

6. Yoshimura Y, Dantzker JLM, Callaway EM. Excitatory cortical neurons form fine-scale functional networks. Nature. 2005; 433:868–873. [PubMed: 15729343]

7. Yoshimura Y, Callaway EM. Fine-scale specificity of cortical networks depends on inhibitory cell type and connectivity. Nat. Neurosci. 2005; 8:1552–1559. [PubMed: 16222228]

8. Lefort S, Tomm C, Floyd Sarria J, Petersen CCH. The excitatory neuronal network of the C2 barrel column in mouse primary somatosensory cortex. Neuron. 2009; 61:301–316. [PubMed: 19186171]

9. Thomson AM, Bannister AP, Mercer A, Morris OT. Target and temporal pattern selection at neocortical synapses. Philos. Trans. R. Soc. Lond., B, Biol. Sci. 2002; 357:1781–1791. [PubMed: 12626012]

10. Holmgren C, Harkany T, Svennenfors B, Zilberter Y. Pyramidal cell communication within local networks in layer 2/3 of rat neocortex. J. Physiol. (Lond.). 2003; 551:139–153. [PubMed: 12813147]

11. Mrsic-Flogel TD, et al. Homeostatic regulation of eye-specific responses in visual cortex during ocular dominance plasticity. Neuron. 2007; 54:961–972. [PubMed: 17582335]

12. Ohki K, Chung S, Ch'ng YH, Kara P, Reid RC. Functional imaging with cellular resolution reveals precise micro-architecture in visual cortex. Nature. 2005; 433:597–603. [PubMed: 15660108]

13. Nimmerjahn A, Kirchhoff F, Kerr JND, Helmchen F. Sulforhodamine 101 as a specific marker of astroglia in the neocortex in vivo. Nat. Methods. 2004; 1:31–37. [PubMed: 15782150]

14. Denk W, Strickler JH, Webb WW. Two-photon laser scanning fluorescence microscopy. Science. 1990; 248:73–76. [PubMed: 2321027]

15. Stosiek C, Garaschuk O, Holthoff K, Konnerth A. In vivo two-photon calcium imaging of neuronal networks. Proc. Natl. Acad. Sci. U.S.A. 2003; 100:7319–7324. [PubMed: 12777621]

16. Jia H, Rochefort NL, Chen X, Konnerth A. Dendritic organization of sensory input to cortical neurons in vivo. Nature. 2010; 464:1307–1312. [PubMed: 20428163]

17. Alonso JM, Martinez LM. Functional connectivity between simple cells and complex cells in cat striate cortex. Nat. Neurosci. 1998; 1:395–403. [PubMed: 10196530]

18. Kohn A, Smith MA. Stimulus dependence of neuronal correlation in primary visual cortex of the macaque. J. Neurosci. 2005; 25:3661–3673. [PubMed: 15814797]

19. Aertsen AM, Gerstein GL, Habib MK, Palm G. Dynamics of neuronal firing correlation: modulation of "effective connectivity". J. Neurophysiol. 1989; 61:900–917. [PubMed: 2723733]

20. Mariño J, et al. Invariant computations in local cortical networks with balanced excitation and inhibition. Nat. Neurosci. 2005; 8:194–201. [PubMed: 15665876]

21. Ben-Yishai R, Bar-Or RL, Sompolinsky H. Theory of orientation tuning in visual cortex. Proc. Natl. Acad. Sci. U.S.A. 1995; 92:3844–3848. [PubMed: 7731993]

22. Douglas RJ, Koch C, Mahowald M, Martin KA, Suarez HH. Recurrent excitation in neocortical circuits. Science. 1995; 269:981–985. [PubMed: 7638624]

23. Li W, Piëch V, Gilbert CD. Contour saliency in primary visual cortex. Neuron. 2006; 50:951–962. [PubMed: 16772175]

24. Alonso JM, Usrey WM, Reid RC. Rules of connectivity between geniculate cells and simple cells in cat primary visual cortex. J. Neurosci. 2001; 21:4002–4015. [PubMed: 11356887]

25. Clopath C, Büsing L, Vasilaki E, Gerstner W. Connectivity reflects coding: a model of voltage-based STDP with homeostasis. Nat. Neurosci. 2010; 13:344–352. [PubMed: 20098420]

26. Tolhurst DJ, Movshon JA, Dean AF. The statistical reliability of signals in single neurons in cat and monkey visual cortex. Vision Res. 1983; 23:775–785. [PubMed: 6623937]

27. Barlow H. Redundancy reduction revisited. Network. 2001; 12:241–253. [PubMed: 11563528]

28. Alitto HJ, Dan Y. Function of inhibition in visual cortical processing. Curr. Opin. Neurobiol. 2010; 20:340–346. [PubMed: 20307968]

29. Marshel JH, Mori T, Nielsen KJ, Callaway EM. Targeting Single Neuronal Networks for Gene Expression and Cell Labeling In Vivo. Neuron. 2010; 67:562–574. [PubMed: 20797534]

30. Denk W, Horstmann H. Serial block-face scanning electron microscopy to reconstruct three-dimensional tissue nanostructure. PLoS Biol. 2004; 2:e329. [PubMed: 15514700]
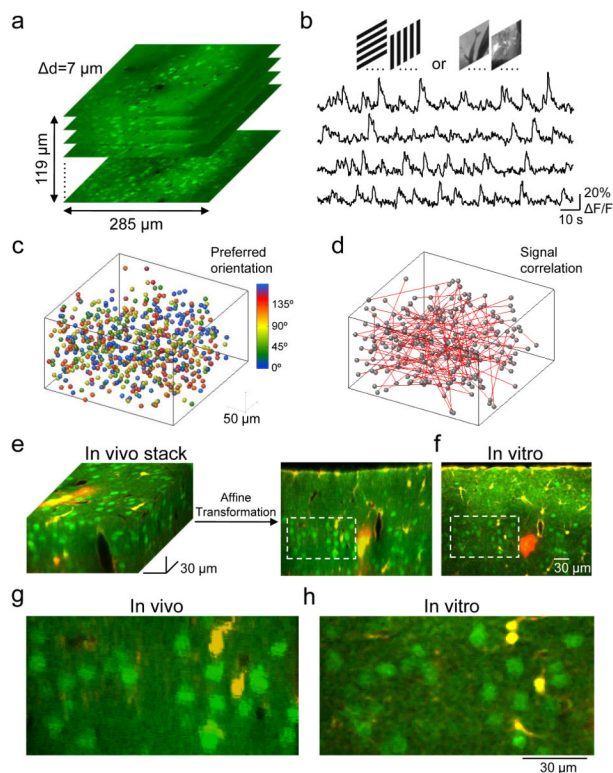
Figure 1. Imaging functional properties of neurons *in vivo* and indentifying the same neurons *in vitro*

a, Two-photon imaging was used to sample somatic calcium signals from a complete population of L2/3 neurons within a $285\times285\times119$ μm^3 volume. Imaging was carried out at 7 μm depth increments. Neurons were labeled with the calcium indicator dye OGB-1 AM (green) and the astrocyte marker SR101 (red). b, Example traces of calcium signals from four different cells in the imaged volume while presenting six trials of grating stimuli drifting in eight different directions. c, All orientation selective cells in the volume were color-coded according to preferred orientation and plotted as spheres. d, Signal correlations were computed from average responses to natural movies. Red lines represent strongly correlated neuronal pairs (signal correlation > 0.2). e and f, After imaging visually evoked calcium signals, a detailed image stack was obtained *in vivo*. The brain was sliced coronally and another stack of the same tissue was obtained *in vitro* (a single optical plane is shown in f). Affine transformation was used to align the *in vivo* to the *in vitro* stack, allowing precise matching of OGB-1-filled cells in the two stacks. g and h, Close-ups of the regions outlined with dashed lines in e and f, respectively.
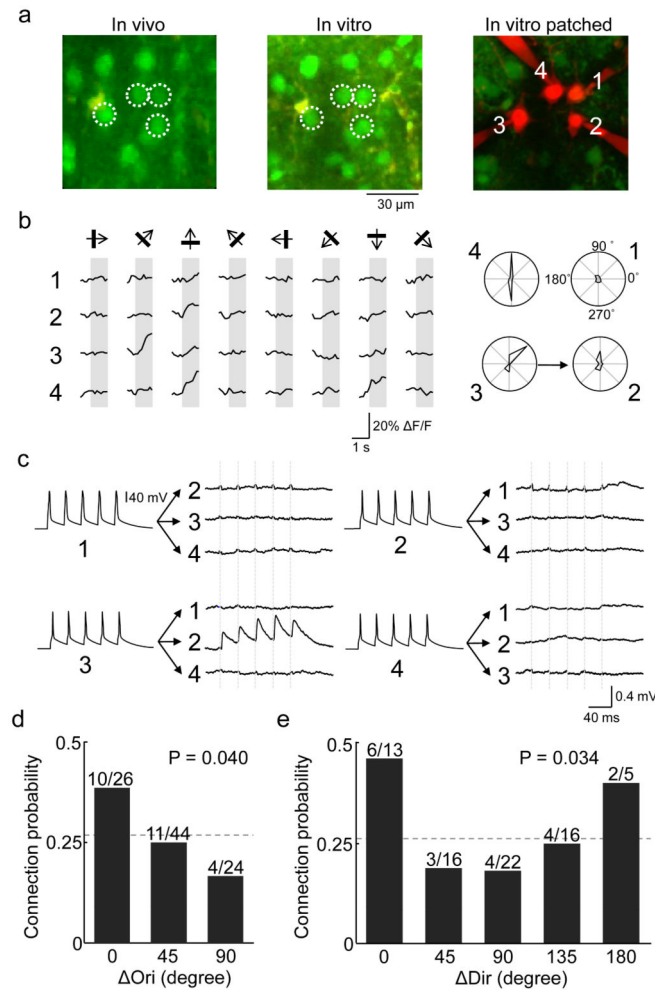
Figure 2. Relating orientation and direction preference to connection probability among L2/3 pyramidal neurons
a White circles denote the locations of *in vivo* to *in vitro* matched cells that were targeted for whole-cell recording and filled with Alexa 594. b. Left: average calcium responses of the four cells to oriented drifting gratings. Right: corresponding polar plots of inferred spike rate responses, normalized to the maximum response of cell 4. Three of the cells (cells 2, 3 and 4) were reliably responsive and orientation selective. Arrow shows a connection detected from cell 3 to cell 2. c, Membrane potential recordings from the four cells. Currents were injected into each cell in sequence, and from average traces of postsynaptic potentials an excitatory connection was found from cell 3 to cell 2. No other connections were found. Vertical dashed lines indicate timing of presynaptic spikes. In some traces, stimulation artefacts are visible that coincided exactly with presynaptic spikes and therefore could be clearly distinguished from EPSPs. d, Relationship between connection probability and difference in preferred orientation (ΔOri) among pairs in which both neurons were responsive to grating stimuli and were orientation selective (OSI > 0.4). There was a significant decreasing trend in connection probability as ΔOri increased (P = 0.040, Cochran-Armitage test). Dotted line indicates connection probability for all pairs included in this analysis (25/94, 0.27). The bins include difference in orientation values of 0 to 22.5° (zero degree bin), 22.5° to 67.5° (45 degree bin), and 67.5° to 90° (90 degree bin). e, Relationship between connection probability and difference in preferred direction (ΔDir) in the subset of neurons which were direction-selective (DSI > 0.3). The same decreasing trend

with respect to ΔOri was detected (P = 0.034, Cochran-Armitage test). Neurons connected with specificity to preferred orientation but not to preferred direction. Dotted line indicates connection probability for all directionally selective pairs (19/72, 0.26). The bins include difference in orientation values of 0 to 22.5° (zero degree bin), 22.5° to 67.5° (45 degree bin), and so on.
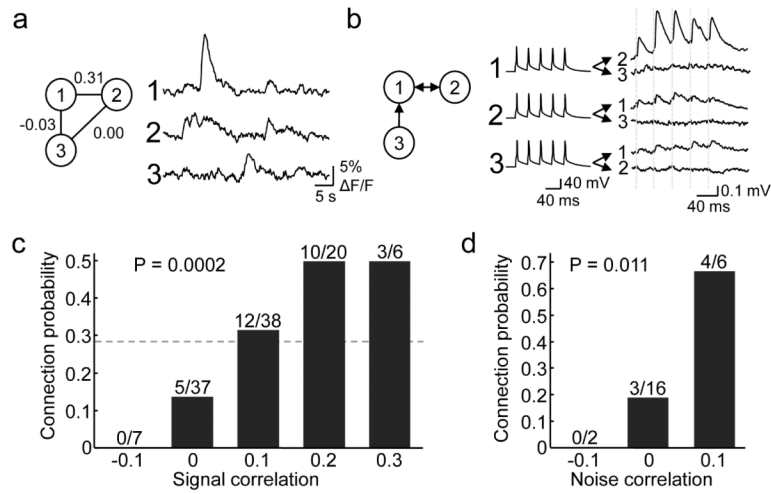
Figure 3. Relationship between response correlation to natural movies and connection probability

a, An example of a triplet of neurons targeted for whole cell recording *in vitro*, with associated *in vivo* calcium responses to the natural movie (average of 6 repetitions) and spike rate correlation values. Neuron 1 and 2 showed correlated firing (signal correlation = 0.31), whereas other pairs did not. b, Triple recordings from the same neurons reveals the pattern of connections: neurons 1 and 2 were bidirectionally connected, while neuron 3 provided input to neuron 1. Dashed lines indicate timing of presynaptic spikes. c, There was a significant increase in connection probability with increasing signal correlation to natural movies (P = 0.0002, Cochran-Armitage test). Dotted line indicates connection probability for all pairs included in this analysis (30/108, 0.28). d, Connection probability increased significantly with increase in noise correlation (P = 0.011, Cochran-Armitage test). Correlation values were binned, with ranges from −0.15 to −0.05, from −0.05 to 0.05, and so on.
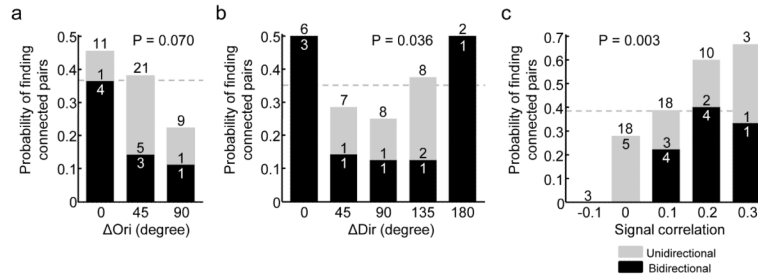
Figure 4. Relationship between similarity of visual responses and probability of finding unidirectionally and bidirectionally connected pairs

a, Among orientation selective neurons, probability of finding connected pairs decreased as ΔOri increased. The fall-off in probability of finding bidirectionally connected pairs was steeper than the decrease in overall probability of finding connected pairs. A trend of decrease in probability of finding bidirectionally connected pairs was found (P = 0.070, Cochran-Armitage test). b, The same observation holds in the subset of directionally selective pairs, and probability of finding bidirectionally connected pairs decreased as ΔOri increased (P = 0.036, Cochran-Armitage test). c, The probability of finding bidirectionally connected pairs increased sharply as signal correlation to natural movies increased (P = 0.003, Cochran-Armitage test). Dotted lines indicate probability of finding connected pairs from all pairs included in analysis (panel a: 15/41, 0.37; panel b: 11/31, 0.35; panel c: 20/52, 0.38).